Supplementary Information (SI) for ChemComm.

Supplementary Materials

Repeatable and renewable synthesis of nickel-iron nitrate hydroxide needle-like arrays for water electrolysis

Experimental section

Materials

All reagents were analytical grade and used without further purification. Ni foam and NiFe foam (labeled as NF and NFF) were purchased from Suzhou Jiashide Co., Ltd. Fe foam (labeled as FF) was purchased from Suzhou Zhengtairong Co., Ltd. Potassium hydroxide (KOH) was purchased from Shanghai Meryer Chemical Technology Co., Ltd. Iron (III) nitrate nonahydrate [$Fe(NO_3)_3 \cdot 9H_2O$] was purchased from Sinopharm Chemical Reagent Co., Ltd. Nickel nitrate hexahydrate [$Ni(NO_3)_2 \cdot 6H_2O$] was purchased from Sinopharm Chemical Reagent Co., Ltd. Ethanol, and acetone were purchased from Beijing Chemical Works. Milli-Q deionized water (resistance of 18.2 MΩ cm at 25 °C) was used for all experiments.

Synthesis of NNO-NFF, NNO-FF, and NNO-NF

The NFF was cut into pieces of 1×4 cm^2 and cleaned ultrasonically in acetone, absolute ethyl alcohol, and deionized water for 10 minutes, then dried in a vacuum oven at 60 °C, respectively for later use. The NNO-NFF was prepared by a low-temperature molten salt strategy. First, an appropriate amount of $Ni(NO_3)_2 \cdot 6H_2O$ is put into a clean glass container and transferred to an oven at 125 °C for 30 min until completely melted. Then a piece of NFF was quickly put into the melted $Ni(NO_3)_2 \cdot 6H_2O$ and kept at 125 °C for 10 h. Then the soaked NFF was taken out and repeatedly rinsed with deionized water to remove excess $Ni(NO_3)_2 \cdot 6H_2O$. Finally, the treated NFF was dried under vacuum at 60℃ for

4h. The samples with reaction time of 0 h, 1 h, 5 h, 12 h, and 15 h were also prepared. The resulting samples were noted as NNO-NFF-0 h, NNO-NFF-1 h, NNO-NFF-5 h, NNO-NFF-12 h, and NNO-NFF-15 h, respectively.

The NNO-FF and NNO-NF were synthesized by the same method using FF and NF as substrates, respectively.

Synthesis of FNO-NFF

The FNO-NFF was prepared using the same method as for NNO-NFF except for replacing the $Ni(NO_3)_2 \cdot 6H_2O$ with $Fe(NO_3)_3 \cdot 9H_2O$. Considering the melting point of different nitrate salts, FNO-NFF was obtained by heating at 75 °C for 1min.

Synthesis of NNO-NFF-ns

For comparison, NNO-NFF-ns (n represents the number of times that nickel nitrate molten salt was reused) was prepared in the same way as NNO-NFF. Specifically, immerse 4 clean 1×4 cm^2 NFF electrodes in nickel nitrate molten salt that has been reused 2, 4, 6, and 8 times, respectively. Allow a reaction to occur at 125 °C for 10 h. Then, remove the electrodes, rinse them thoroughly with deionized water, and dry them in a vacuum at 60 °C for 4 h to obtain the final electrodes. These samples are designated as NNO-NFF-3s, NNO-NFF-5s, NNO-NFF-7s, and NNO-NFF-9s, respectively.

Synthesis of NNO-NFF-after regeneration

An appropriate amount of deionized water was added into the nickel nitrate molten salt that was reused 9 times. Then it was maintained in an oven at 50 ℃ for 96 h after being stirred evenly. Thus, the regeneration was carried out to obtain the refreshed

$Ni(NO_3)_2$. The NNO-NFF-after regeneration electrode was prepared by the same process as NNO-NFF, except using the refreshed $Ni(NO_3)_2$ as molten salt. To elaborate, place the clean 1×4 cm^2 NFF electrode into the refreshed $Ni(NO_3)_2$ molten salt, etch it at 125 °C for 10 h, then remove the electrode, rinse it repeatedly with deionized water to remove excess nickel nitrate molten salt from the surface, and vacuum dry it at 60 °C for 4 h to obtain the final electrode, which is named NNO-NFF-after regeneration.

Materials Characterizations

The morphology of the electrodes was observed by Zeiss Ultra 55 field emission scanning electron microscope (SEM), and elemental analysis was performed by energy dispersive X-ray (EDX) spectrum. Transmission electron microscopy (TEM, JAPAN-JEOL-JEM 2100 F), High-resolution TEM (HRTEM), and selected area electron diffraction (SAED) images were characterized at 200 kV accelerating voltage. The X-ray photoelectron spectroscopy (XPS) analysis was carried out on ESCALab MKII spectrometer, which uses Mg Ka X-ray as the source of excitation. In our study, all samples were placed in clear sealed glass bottles. The prepared sample is immediately analyzed, avoiding contamination of the sample during storage. X-ray diffraction (XRD) was performed by using a Rigaku SmartLab, operated at 40 kV and 44 mA, parallel beam mode, λ=1.54 Å, and scan rate 5 degree/min to investigate the crystal structure of electrodes.

Electrochemical Measurement

All electrochemical tests were carried out with CHI 660E. Hg/HgO was used as the reference electrode and Pt mesh as the counter electrode. The scanning rate of linear scanning voltammetry (LSV) was 5 mV s^{-1}. Measurements were conducted in 1 M KOH solution, and the working electrode was controlled at 1×1 cm. All of the measured potentials (vs.Hg/HgO) were converted to the potentials against the reversible hydrogen electrode (RHE) by Nernst equation $E_{RHE}=E_{Hg/HgO}+0.098+0.0591\times pH$. Electrochemical impedance spectroscopy (EIS) data were collected from 100 kHz to 0.01 Hz at overpotentials of 250 mV with an AC amplitude of 5 mV. The electrochemical active surface area (ECSA) curve was measured by different scanning rates (50, 60, 70, 80, and 100 mV s^{-1}). There was no Faraday reaction in the voltage range from 0.724 V to 0.824 V. The capacitive current of the cyclic voltammetry curve ($\Delta J|Ja-Jc|/2$) was drawn to fit the double-layer capacitance (C_{dl}), which is proportional to the surface area of the electrode.

All presented potentials were corrected against the ohmic potential drop with 85% iR compensation.

Supplementary Figures

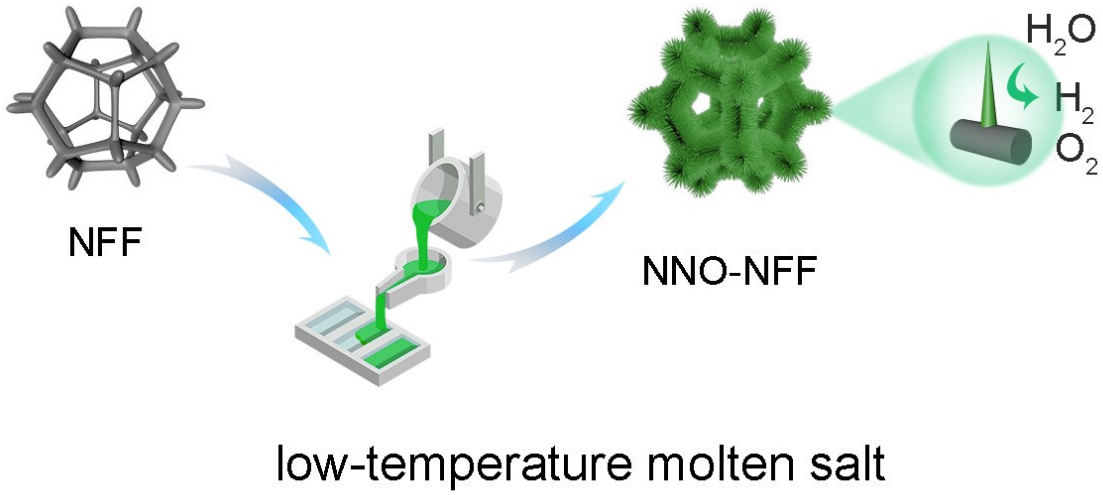

Fig. S1 Schematic Diagram of the Synthesis of NNO-NFF.

NiFe nitrate hydroxide needle-like arrays were synthesized using a straightforward low-temperature molten salt method, utilizing existing nickel nitrate molten salt as the medium and NiFe foam as the solid reaction source. In principle, the possible formation process of $Ni_2(NO_3)_2(OH)_2$ can be hypothesized as follows:[1, 2]

$$4Ni(NO_3)_2 \cdot 6H_2O(l) \rightarrow 2Ni_2(NO_3)_2(OH)_2(s)+4NO_2(g)+22H_2O(g)+O_2(g)$$

$$Fe \xrightarrow{NO_3^-} Fe^{2+} + 2e^-$$

$$Fe^{2+} \xrightarrow{O_2} Fe^{3+} + e^-$$

In molten $Ni(NO_3)_2$, the Fe atoms from the metallic NiFe foam tends to release into the ion liquid to form Fe^{2+} and Fe^{3+} with the help of NO_3^- and O_2.[3, 4] The resultant Fe^{2+} and Fe^{3+} then move freely and rapidly in the solution, attacking the lattice planes of $Ni_2(NO_3)_2(OH)_2$, thereby realizing Fe doping.

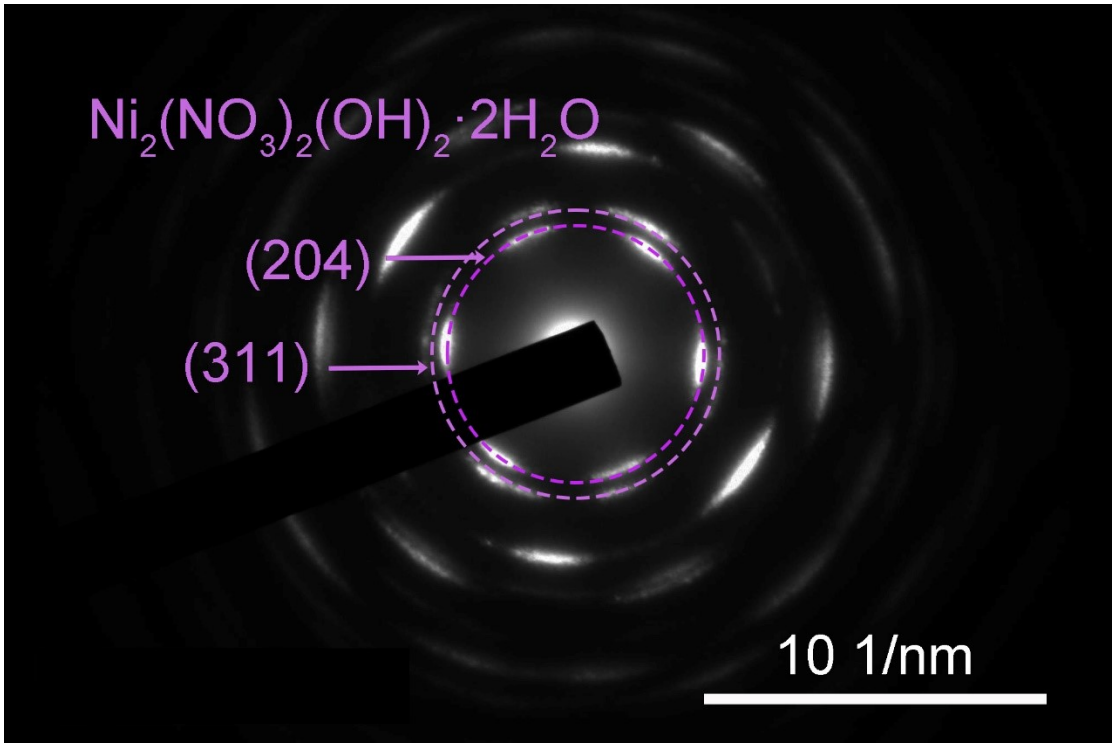

Fig. S2. The SAED image of the NNO-NFF.

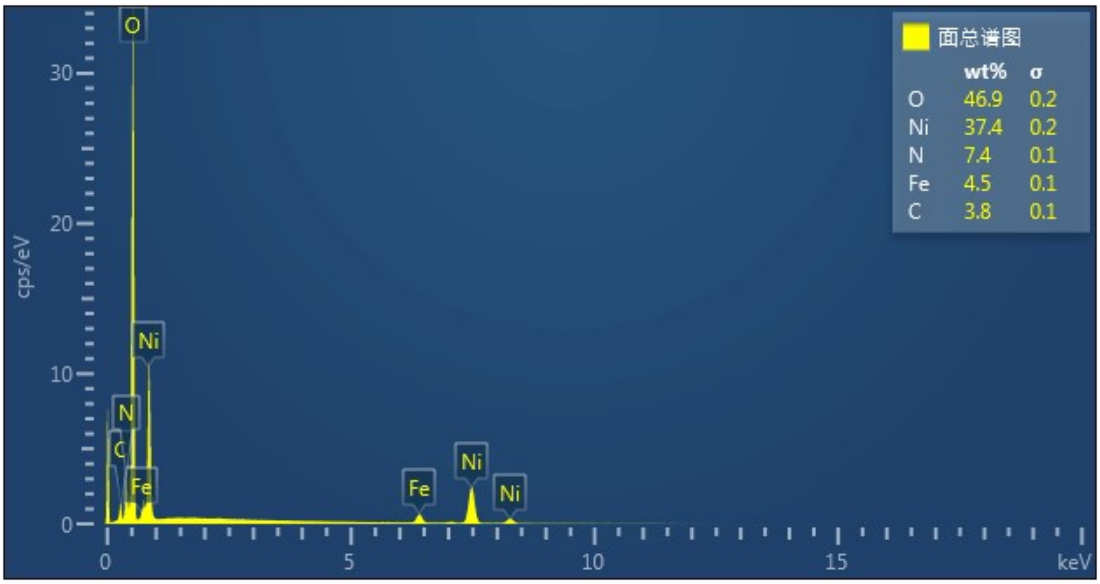

Fig. S3. Element mass distribution of the NNO-NFF.

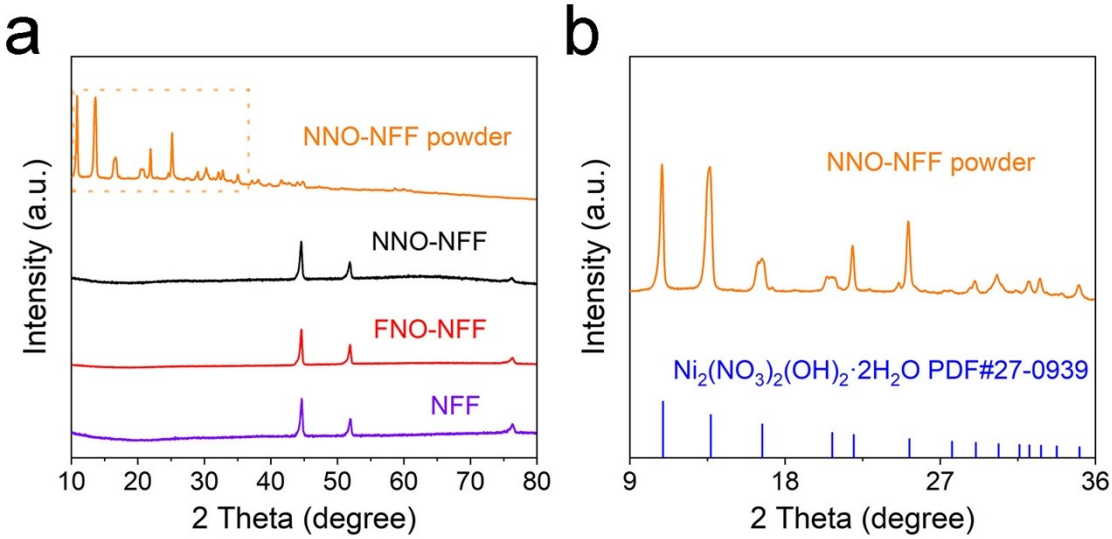

Fig. S4. XRD patterns of the bare NFF, FNO-NFF, NNO-NFF, and NNO-NFF powder.

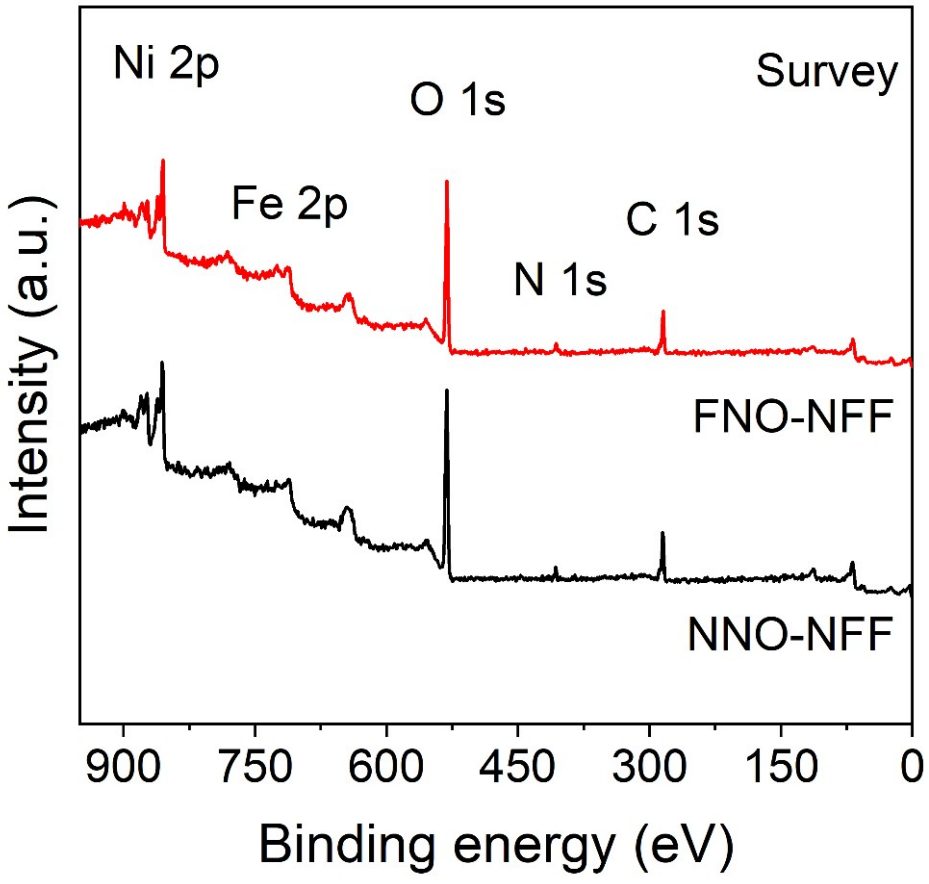

Fig. S5. XPS survey spectrum of NNO-NFF and FNO-NFF.

As depicted in Fig. S5, the survey spectra confirm that the FNO-NFF is composed of Fe, Ni, N, and O. A pair of Ni $2p_{3/2}$ characteristic peaks at 855.8 and 873.5 eV are

attributed to Ni^{2+}, confirming that the synthesized sample is nickel hydroxide rather than oxide (Fig. 2a).[5] The $2p_{3/2}$ and $2p_{1/2}$ peaks appeared owing to a spin-orbit coupling phenomenon that split the Ni 2p peak into a doublet with a peak-to-peak separation of 17.7 eV, as observed earlier for $Ni(OH)_2$ compounds.[6] In the Fe 2p spectrum for FNO-NFF (Fig. 2b), the binding energy of 706.1 eV corresponds to Fe^0. Fe $2p_{3/2}$ peaks are attributed to Fe^{2+} (711.3 eV) and Fe^{3+} (713.8 eV), and Fe $2p_{1/2}$ peaks correspond to Fe^{2+} (723.9 eV) and Fe^{3+} (726.6 eV), respectively.[7] The N 1s peak at 406.8 eV can be assigned to NO_3^- in Fig. 2c.[2] For the O 1s region in Fig. 2d, 530.0 eV, 531.2 eV, and 532.2 eV belong to M-O, M-OH, and adsorbed water, respectively.[8]

Compared to FNO-NFF, the Ni 2p XPS spectrum of NNO-NFF exhibits a negative shift of 0.1 eV (Fig.2a), whereas the binding energy of Fe 2p experiences a negative shift of 0.4 eV (Fig.2b). This suggests that the Fe (Ni) hydroxide network, in which NO^-_3 is embedded, gives rise to pronounced electronic interactions between Fe and Ni ions.[9] Besides, NNO-NFF has more M-O bond than FNO-NFF (Fig.2d).

According to previous research, the nickel hydroxide nitrate owns the advantages of rich Ni–O bonds and large interlayer spacing, thus storing more electrolyte ions to generate electrochemical activity.[10, 11] Many studies have shown that the formation of NO_3^- anion embedded in $Ni(OH)_2$ structure is very beneficial to improve the electrochemical performance.[12, 13]

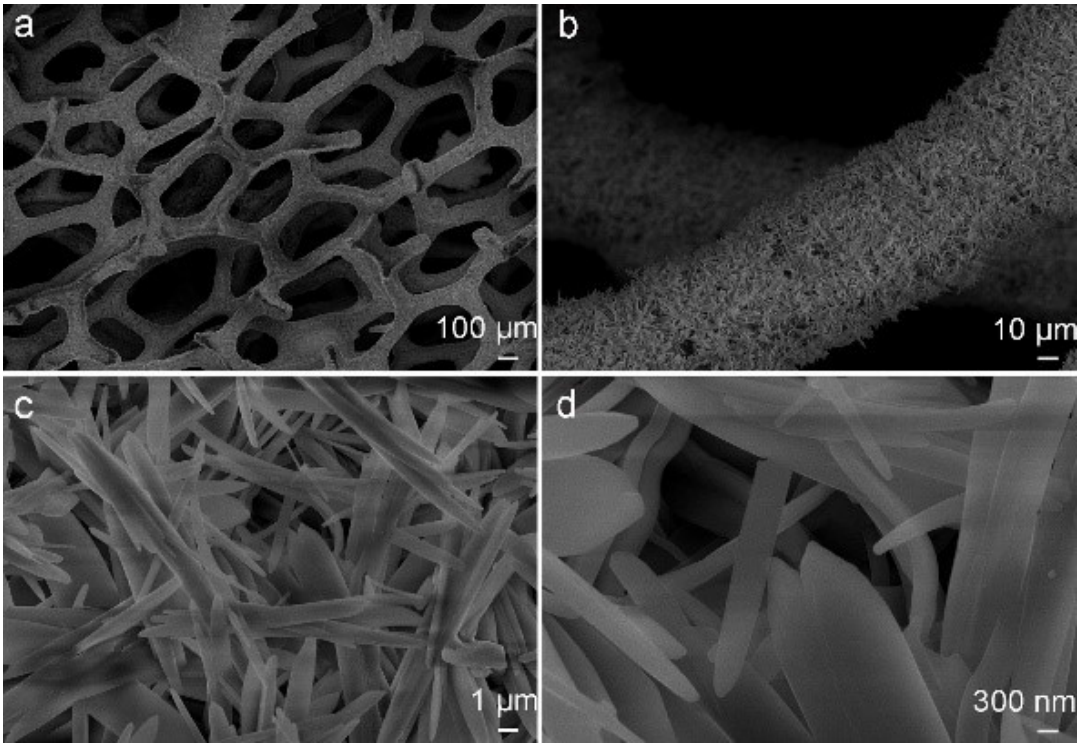

Fig. S6. The SEM images of NNO-NF.

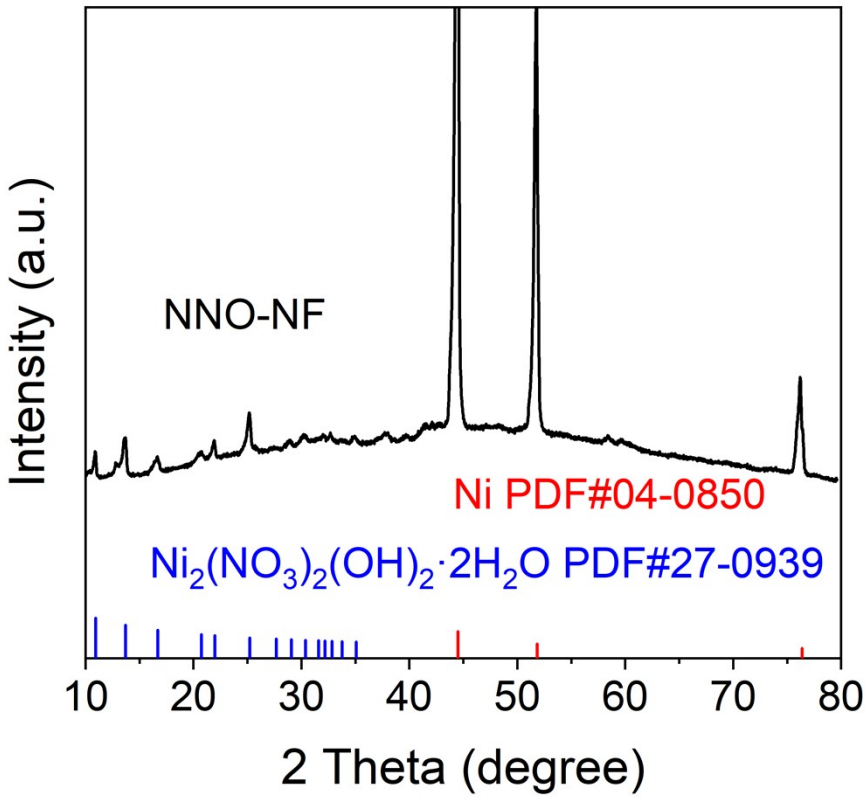

Fig. S7. XRD patterns of the NNO-NF.

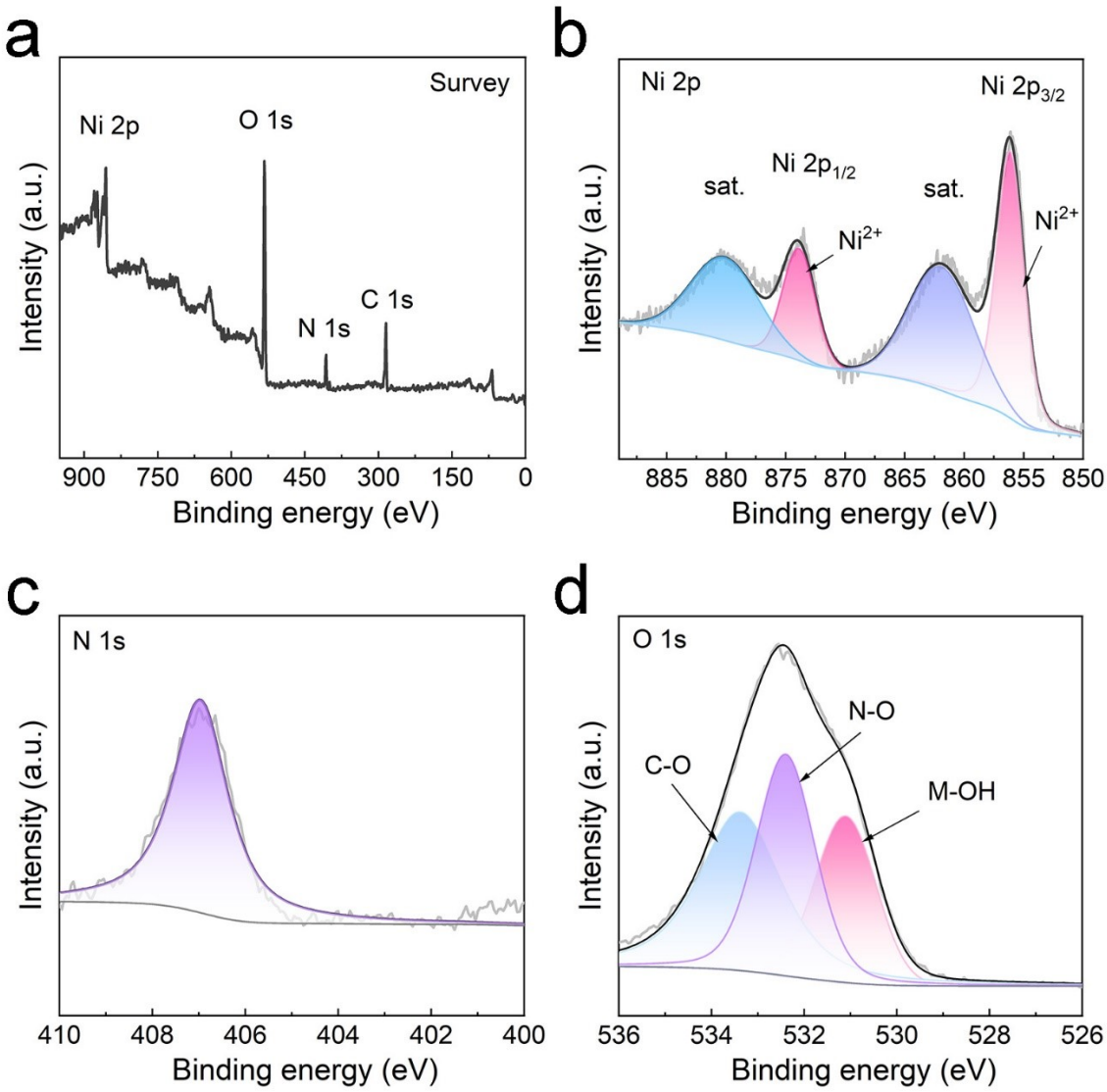

Fig. S8. (a) XPS survey spectrum of the NNO-NF. XPS spectra of (b) Ni 2p, (c) N 1s, and (d) O 1s for the NNO-NF.

Furthermore, XPS was carried out to investigate the elemental composition and chemical states of NNO-NF (Fig. S8). The peaks at 856.1 and 873.8 eV accompanied by two satellite peaks at 861.9 and 880.1 eV are attributed to Ni^{2+} $2p_{3/2}$ and Ni^{2+} $2p_{1/2}$ in NNO-NF, respectively. Consistently, the symmetric N 1s peak at 406.9 eV (Fig. S8c) can be assigned to NO_3^-.[14] The O 1s peak (Fig. S8d) can be deconvoluted into three components: The O-C band (533.3 eV), the O-N band (532.4 eV), and the O-H bond (531.1 eV). A small peak at a higher binding energy of approximately 532.5−533.5 eV is attributed to unavoidable surface physically adsorbed/residual water molecules

and/or carbon−oxygen bond in contaminated organic carbon.[15] These results strongly indicate that NNOH has been successfully prepared on the NF surface.

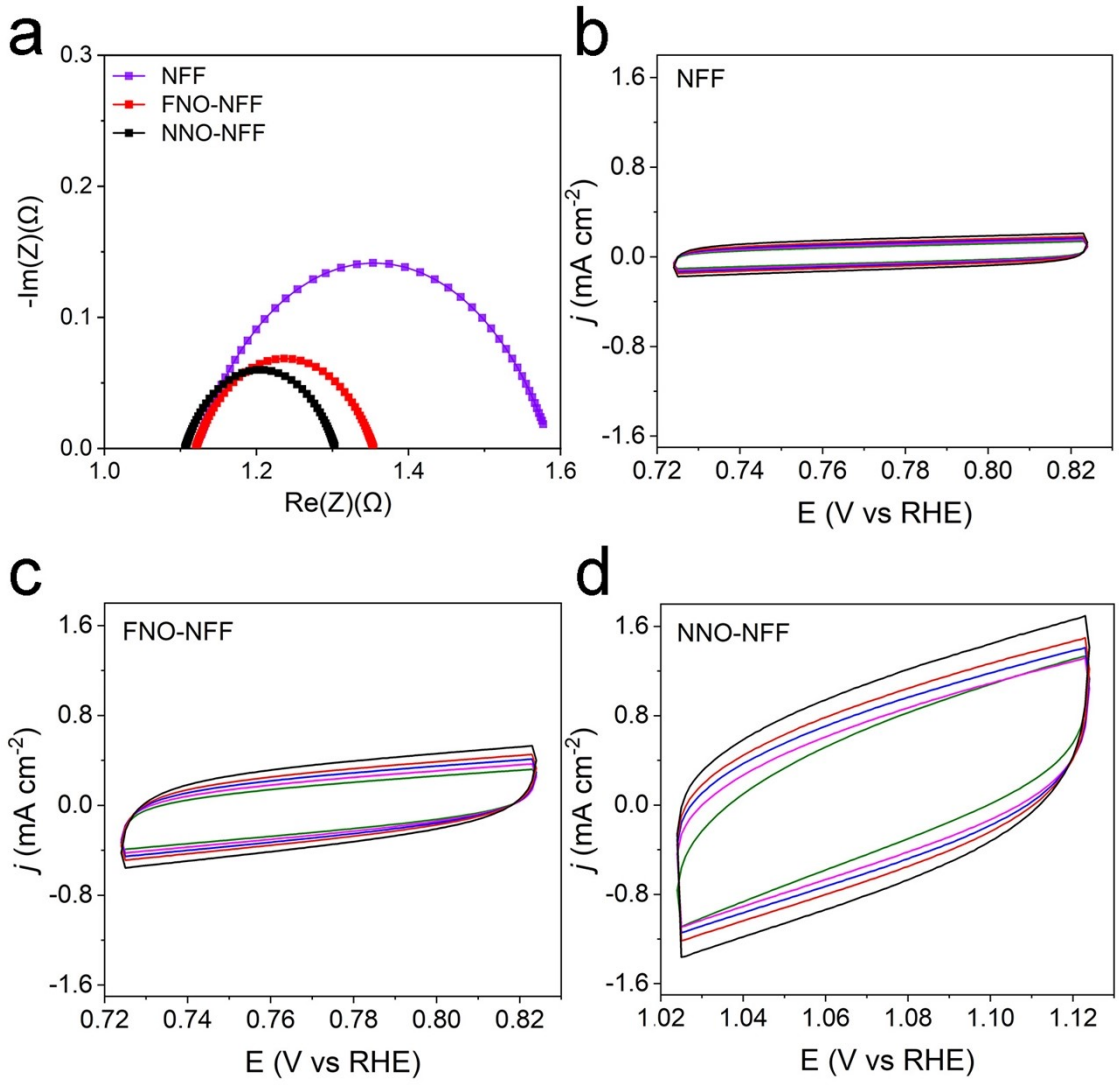

Fig. S9. (a) Nyquist plots of different electrodes for OER. CV curves of (b) NFF, (c) FNO-NFF, (d) NNO-NFF.

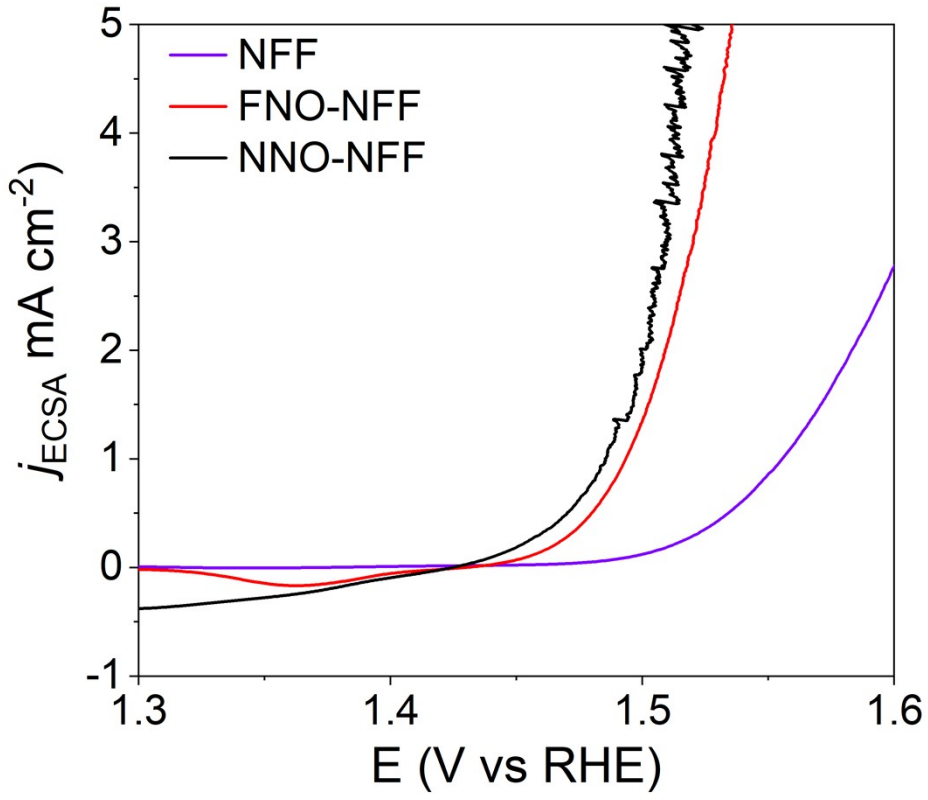

Fig. S10. ECSA-normalized LSVs for OER. ECSA is calculated according to the following equation: ECSA = C_{dl}/C_s, Cs is the specific capacitance of the corresponding surface smooth sample under the same conditions, 40 μF cm^{-2}.[16]

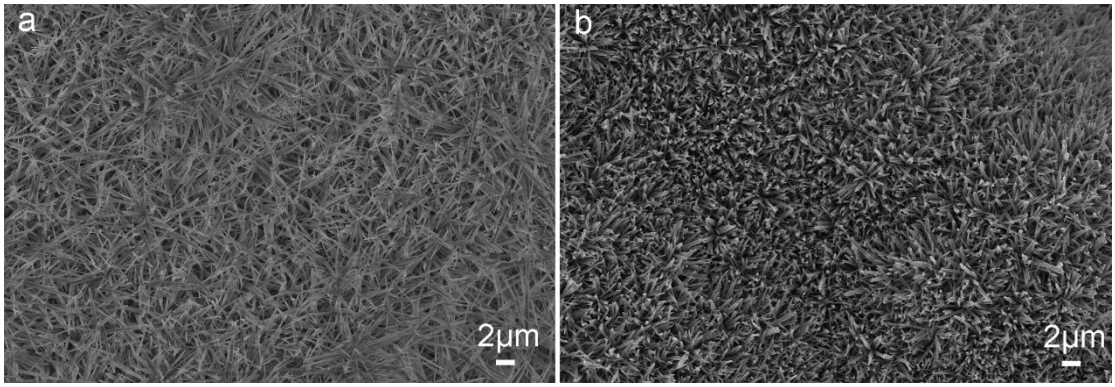

Fig. S11. The SEM images of the NNO-NFF (a) before the OER stability test, (b)after the OER stability test.

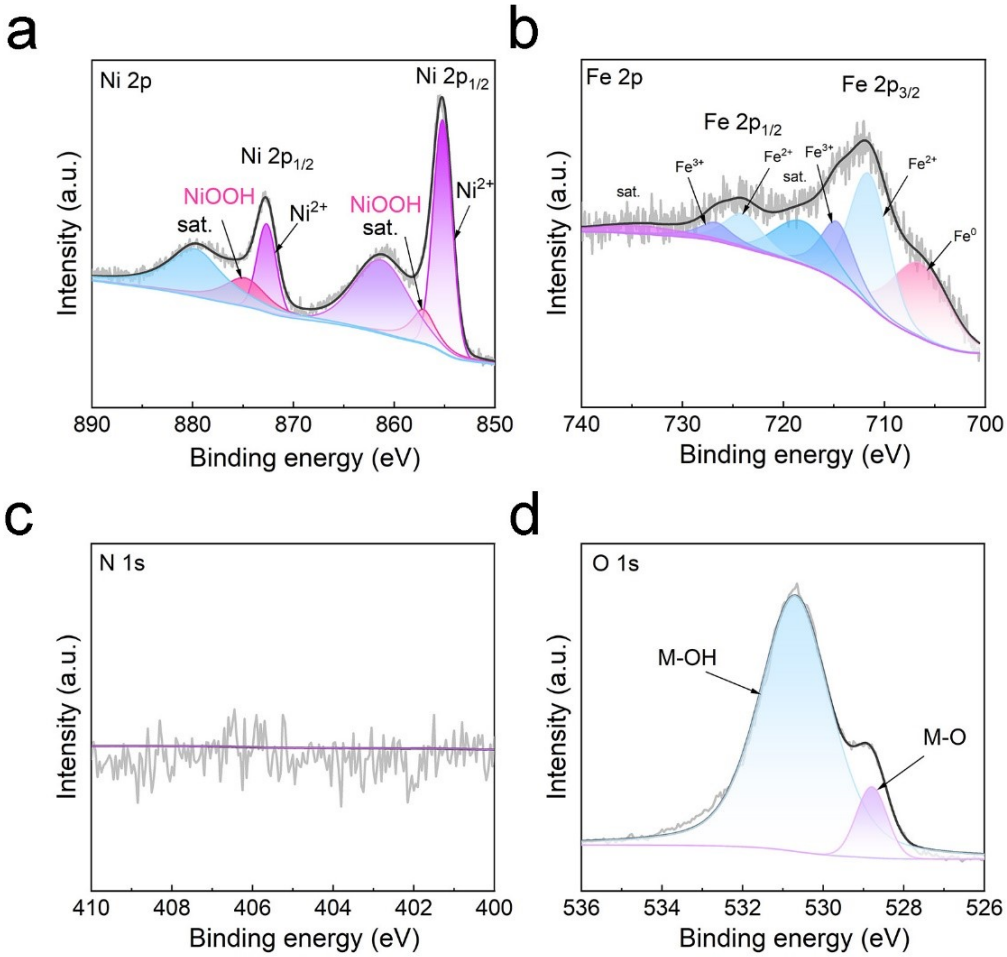

Fig. S12. XPS data of NNO-NFF after the OER stability test.

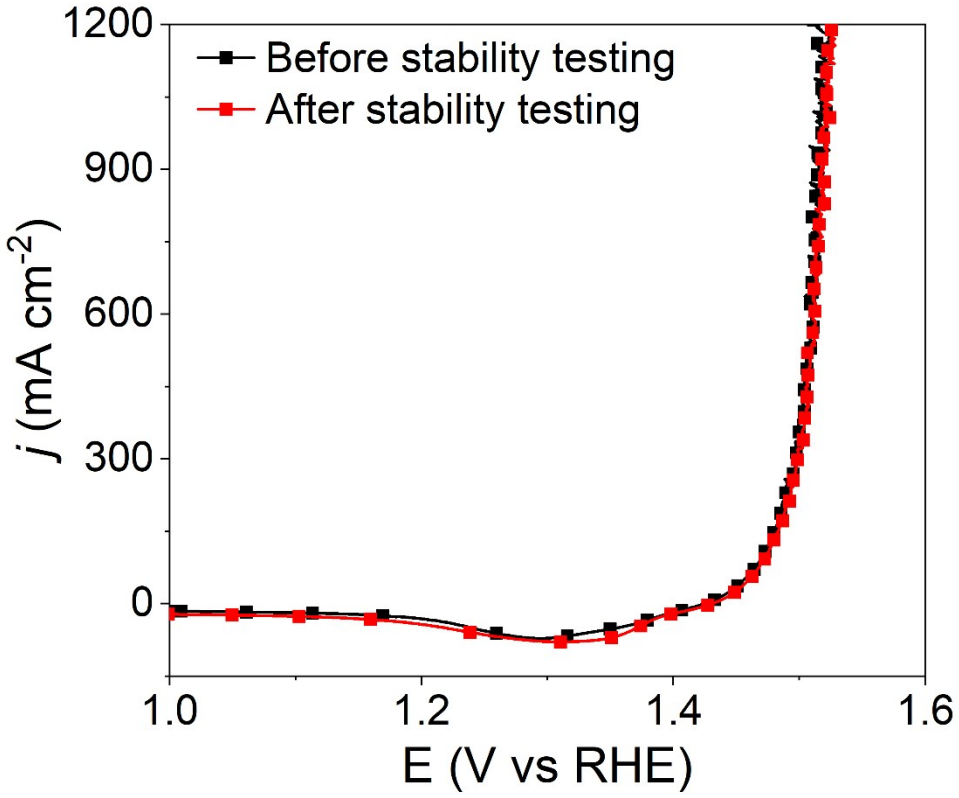

Fig. S13. The LSV curve of NNO-NFF before and after the OER stability test.

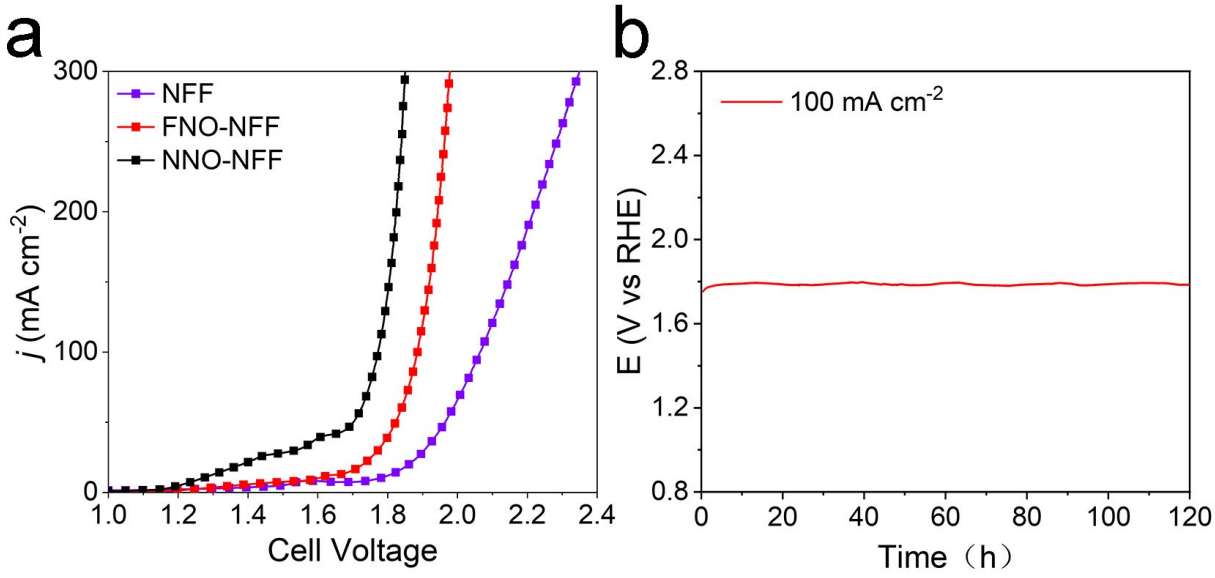

Fig. S14. (a) Polarization curves for overall water splitting in 1 M KOH and (b) CP stability test of NNO-NFF at the current density of 100 mA cm^{-2}.

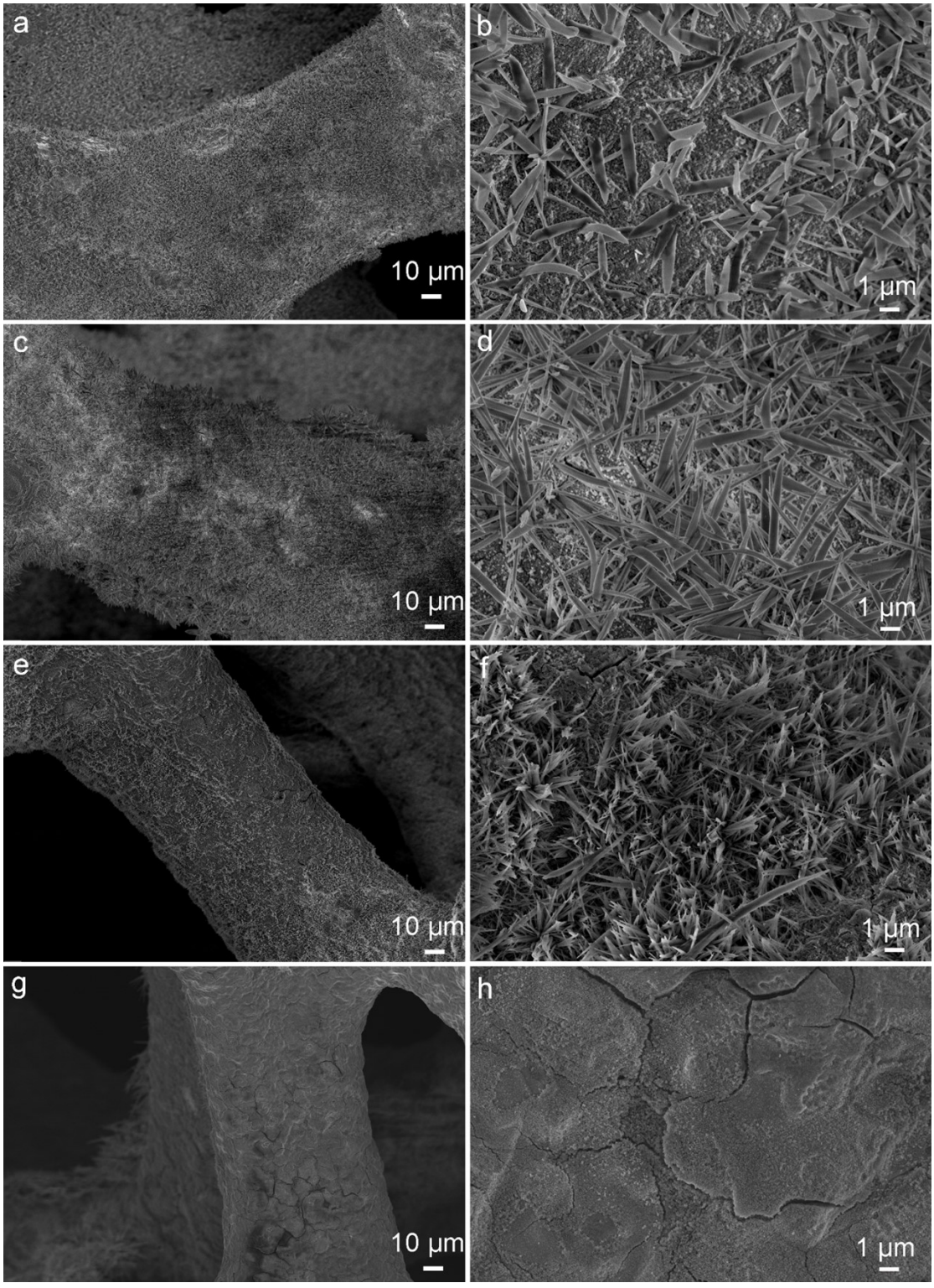

Fig. S15. The SEM images of (a and b) NNO-NFF-1 h, (c and d) NNO-NFF-5 h, (e and f) NNO-NFF-12 h, and (g and h) NNO-NFF-15 h.

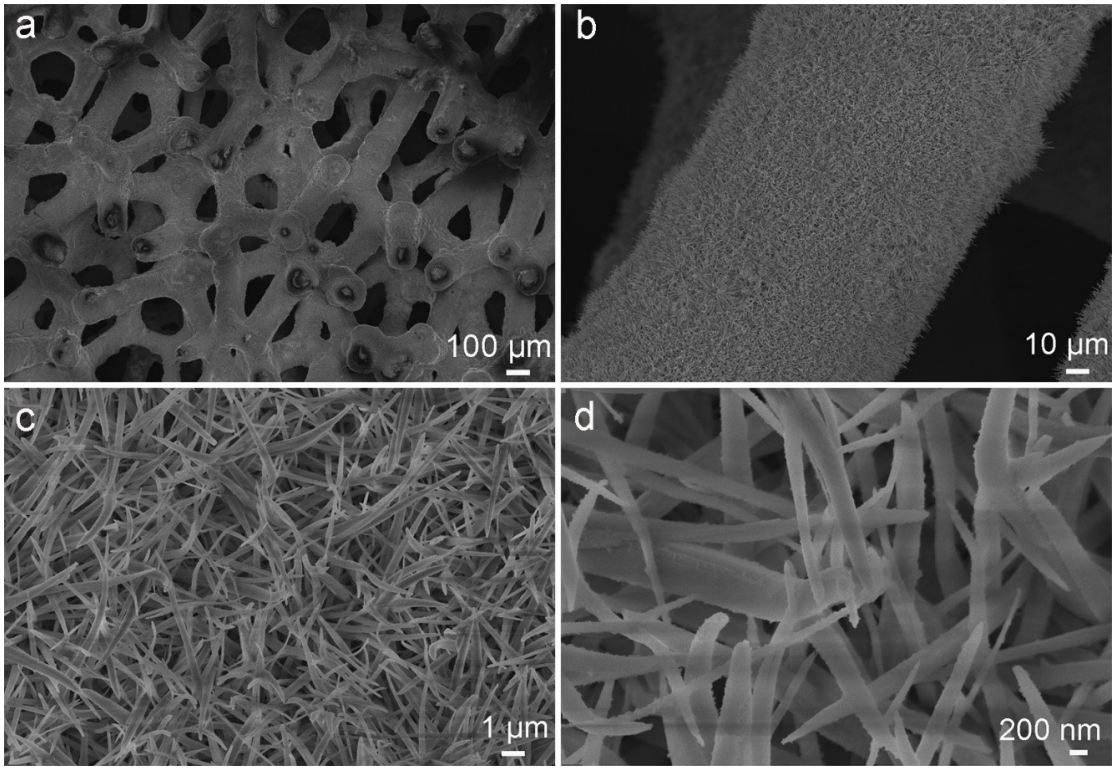

Fig. S16. The SEM images of NNO-NFF.

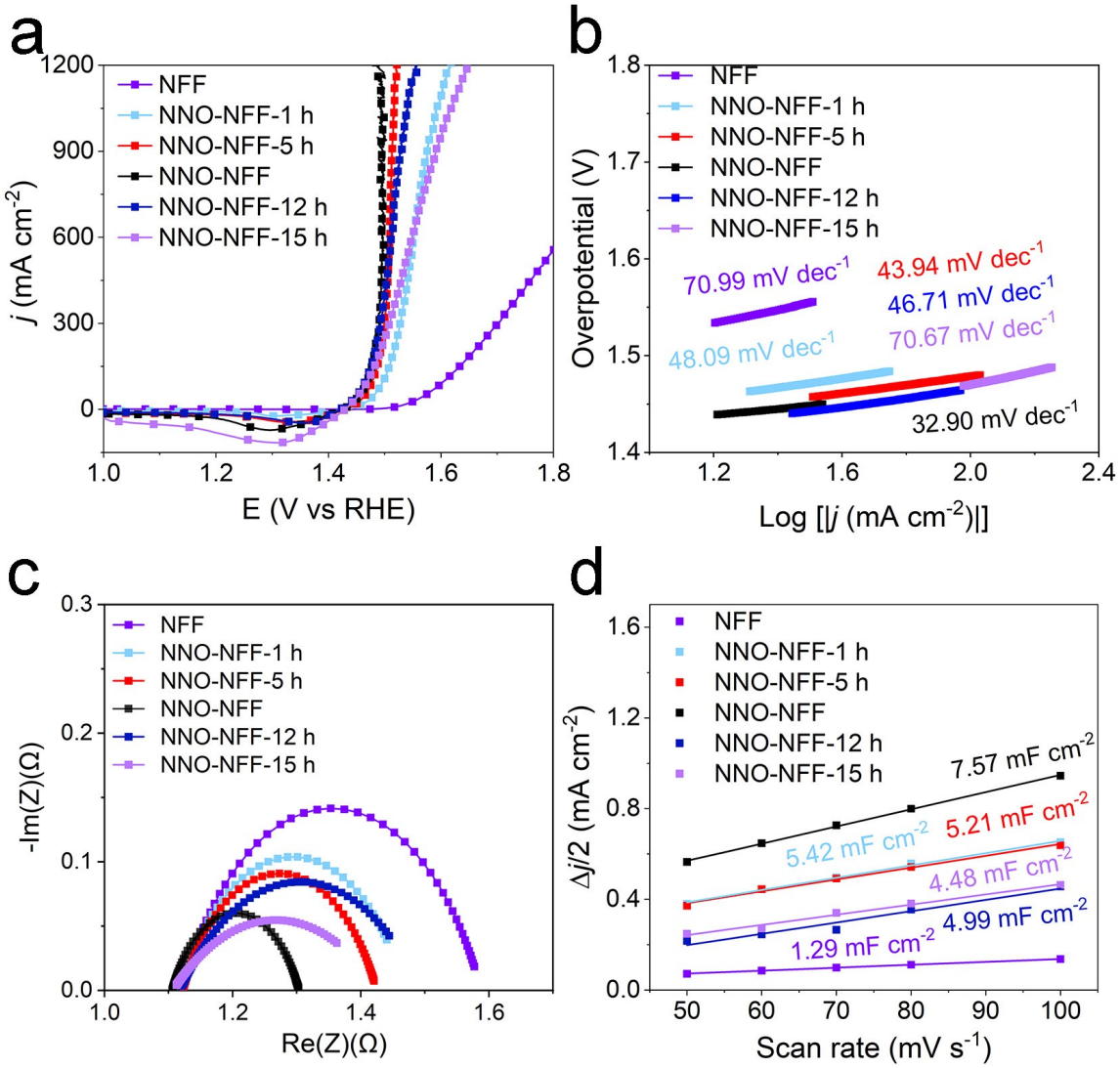

Fig. S17. Electrochemical performance for NFF, NNO-NFF-1h, NNO-NFF-5 h, NNO-NFF, NNO-NFF-12 h and NNO-NFF-15 h. (a) OER, (b) Tafel plots, (c) EIS plots, and (d) C_{dl} plots.

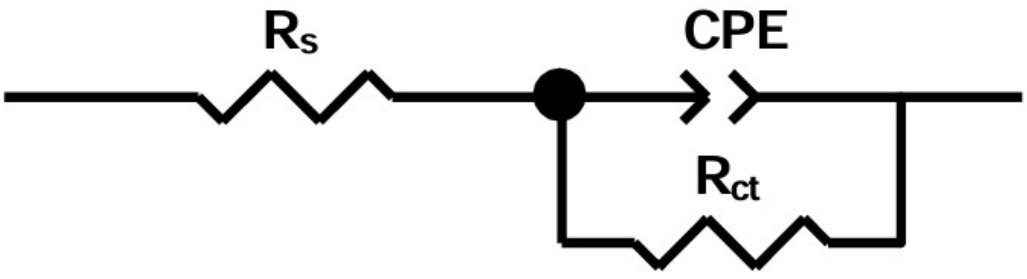

Fig. S18. Equivalent circuit used in the fitting of the impedance data of all samples. R_s: equivalent series resistance, R_{ct}: charge-transfer resistance, CPE: constant-phase element.

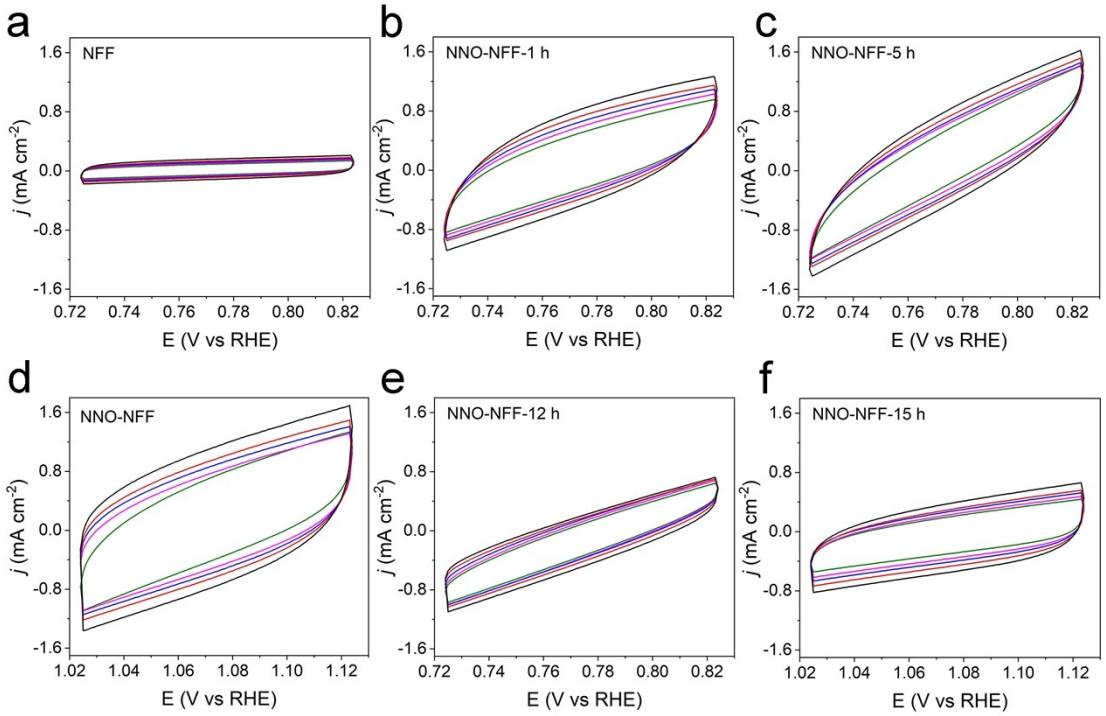

Fig. S19. CV curves of (a) NFF, (b) NNO-NFF-1 h, (c) NNO-NFF-5 h, (d) NNO-NFF, (e) NNO-NFF-12 h, and (f) NNO-NFF-15 h.

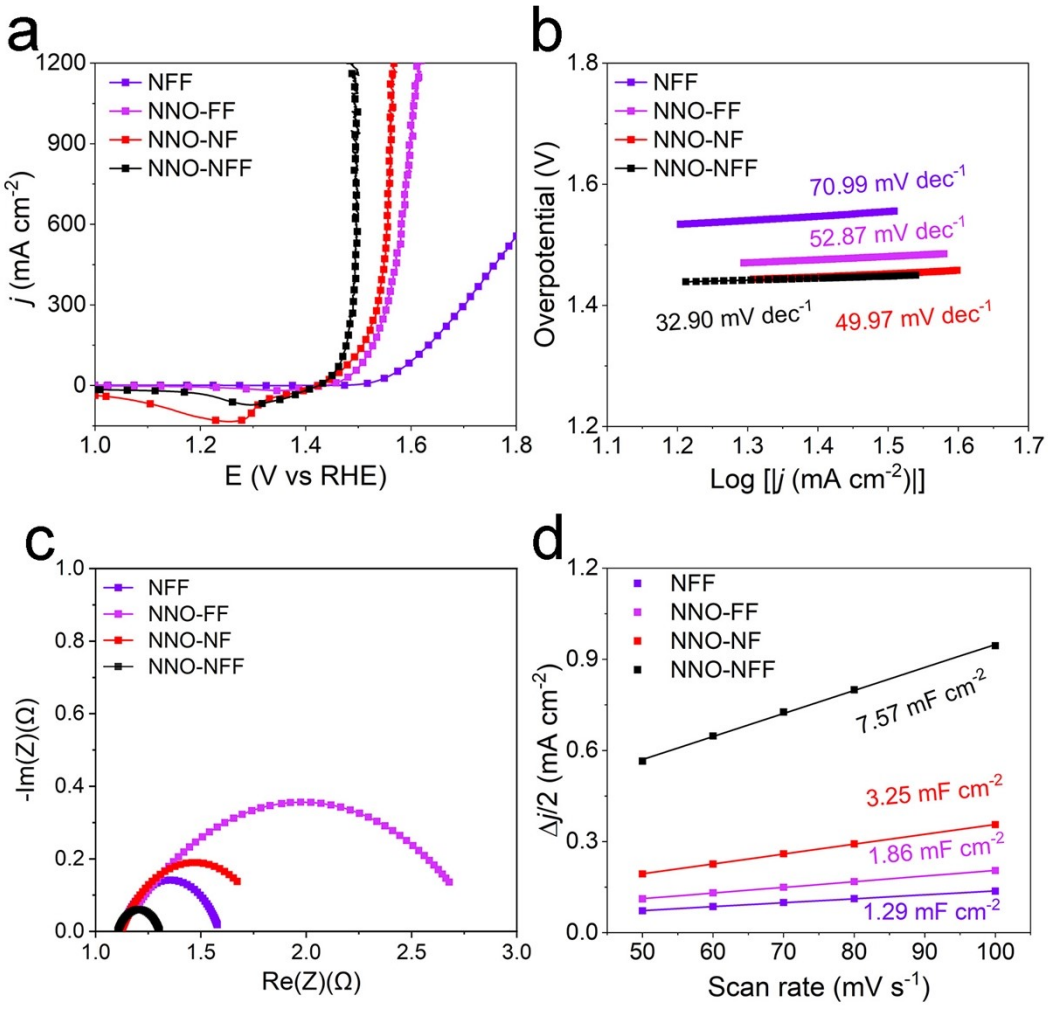

Fig. S20. Electrochemical performance for NFF, NNO-FF, NNO-NF and NNO-NFF. (a) OER, (b) Tafel plots, (c) EIS plots, and (d) C_{dl} plots.

As shown in Fig. S20a, for high current densities of 100 mA cm^{-2}, 500 mA cm^{-2}, and 1000 mA cm^{-2}, the required overpotential for NNO-NFF is 241 mV, 276 mV, and 287 mV, respectively, which is much lower than that for NNO-NF (260 mV, 322 mV, and 330 mV) and NNO-FF (283 mV, 344 mV, and 374 mV). In addition, NNO-NFF has the lowest Tafel slope and the lowest charge transfer resistance (R_{ct} = 0.20 Ω), indicating the fastest OER kinetics compared with the electrodes prepared with single metal foam substrates (Fig. S20b and c).[17] Meanwhile, the C_{dl} value of NNO-NFF is 7.57 mF cm^{-2}, which is 2.33 times and 4.07 times higher than that of NNO-NF and NNO-FF, respectively. (Fig. S20d and S21).

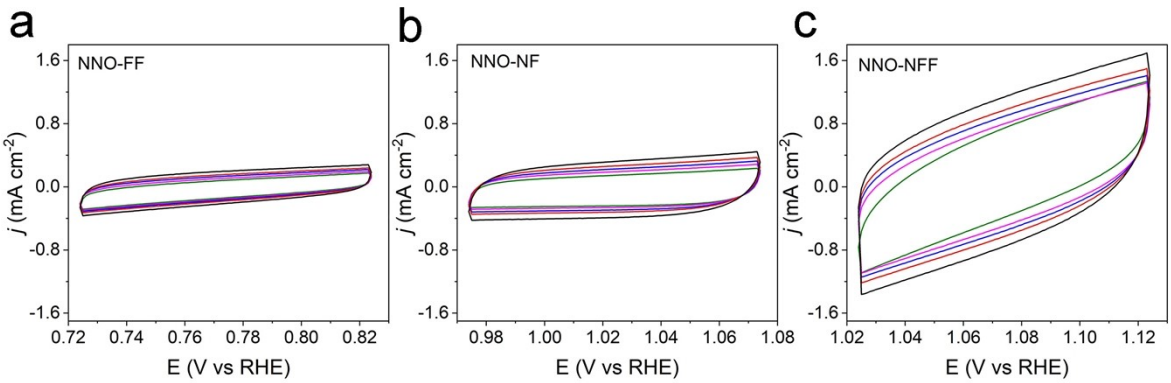

Fig. S21. CV curves of (a) NNO-FF, (b) NNO-NF, (c) NNO-NFF.

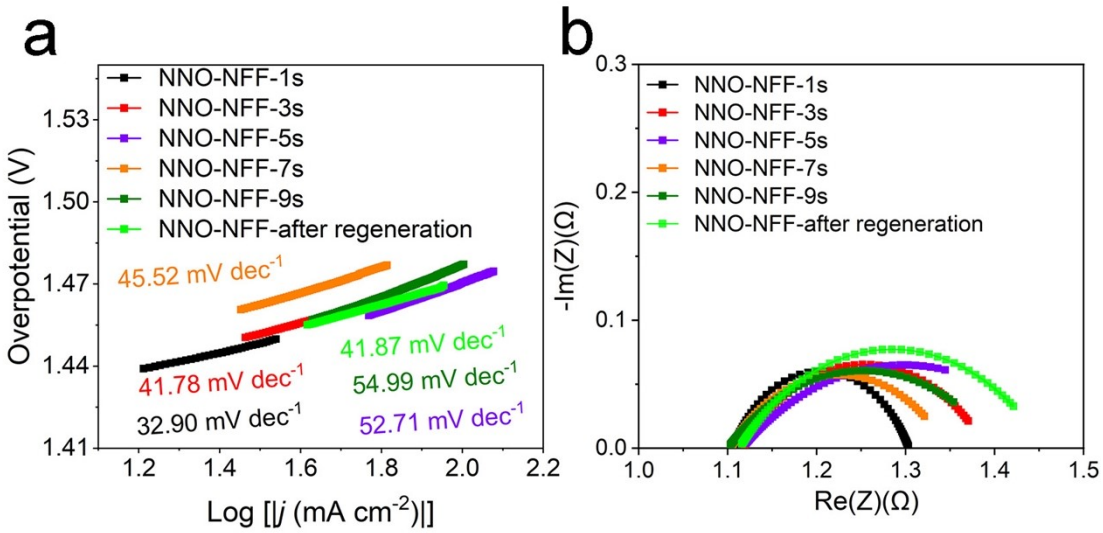

Fig. S22. NNO-NFF-ns and NNO-NFF-after regeneration of (a) Tafel plots, (b) Nyquist plots.

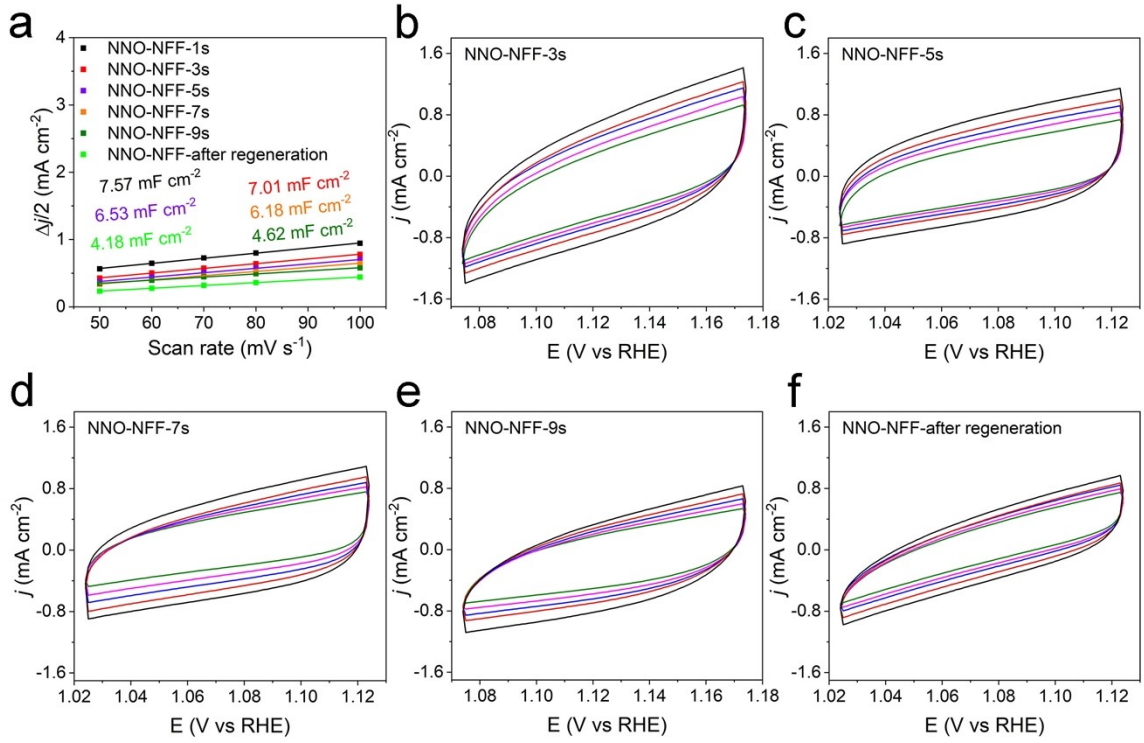

Fig. S23. NNO-NFF-ns and NNO-NFF-after regeneration of (a) C_{dl} plots, (b-f) CV curves.

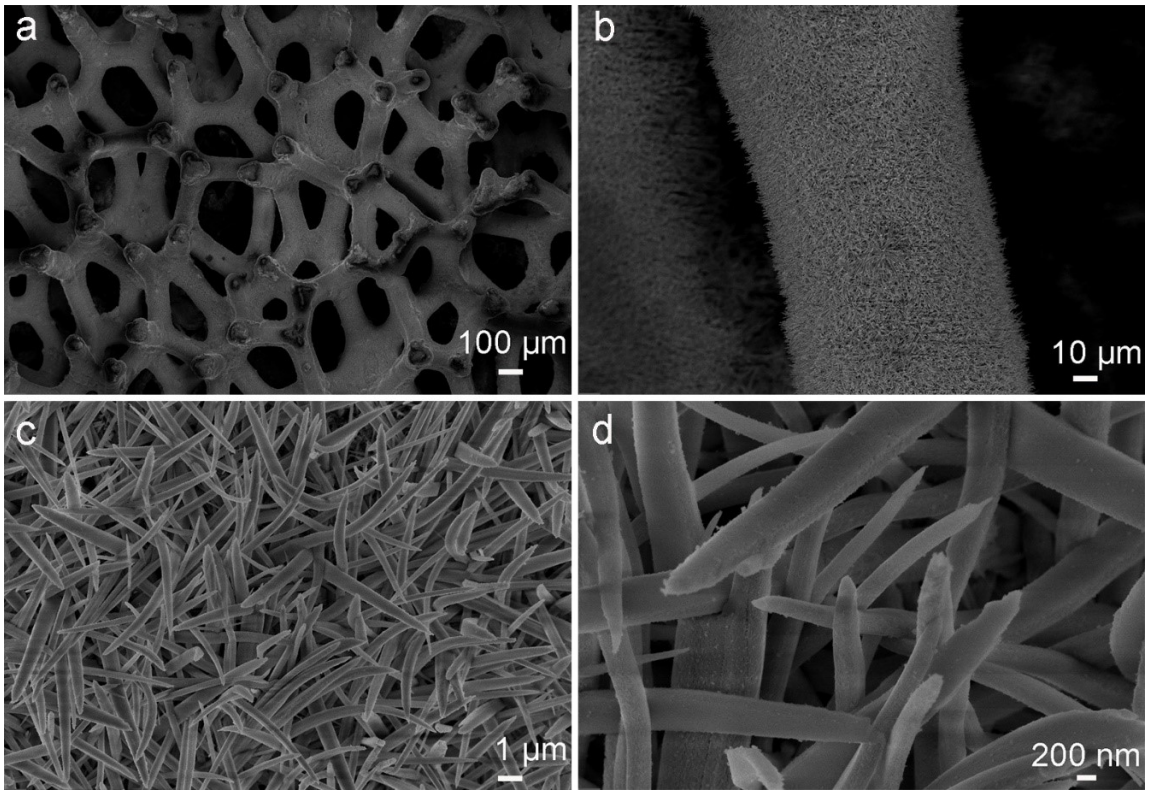

Fig. S24. The SEM images of NNO-NFF-after regeneration.

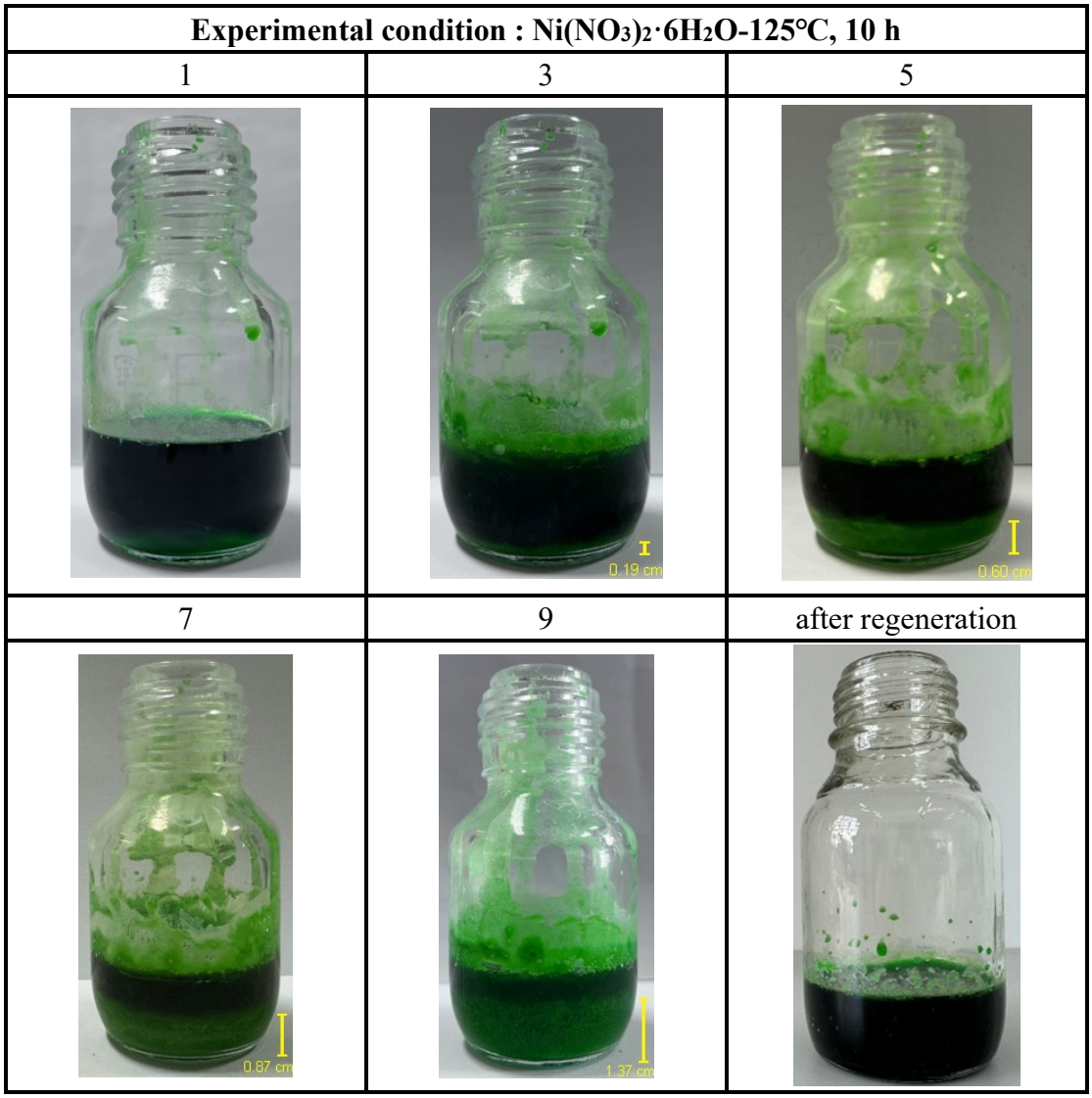

Fig. S25. Optical picture of NNO molten salt at 125℃ with different repetition times.

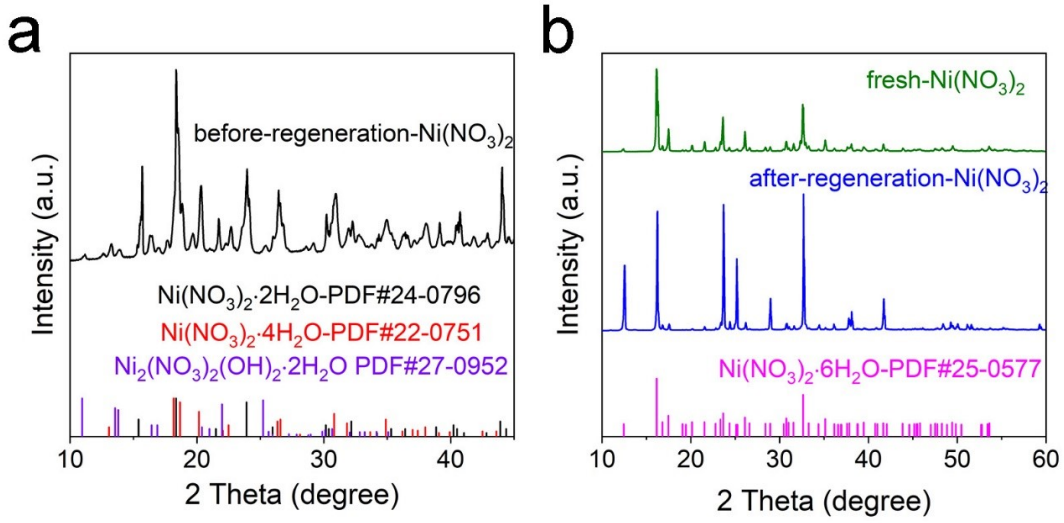

Fig. S26. XRD pattern of NNO molten salt before and after regeneration.

Supplementary Tables

Tab. S1. Comparison the OER performance of NNO-NFF electrode to several recently reported electrocatalysts.

Catalyst	Electrolyte	Overpotential at 100 mA cm^{-2} (mV vs RHE)	Reference
NNO-NFF	1M KOH	241	This work
NiFe LDH-SnO_2/NF	1M KOH	249	18
A-NiFeV/NF	1M KOH	313	19
FeCoNiMo HEA/C	1M KOH	300	20
NiFe-BPDC MOFs/NF	1M KOH	288	21
MIL-53(Fe)/MoS_2/NF	1M KOH	280	22
NiFe-LDH/MoS_2–Ni_3S_2/NF	1M KOH	347	23
Ni_3S_2/ZrCoFe-LDH-NF	1M KOH	330	24
NiFeLDH/$Mo_{4/3}B_{2-x}T_z$/NF	1M KOH	255	25
CoMoP-FexP/NF	1M KOH	290	26
NiFeCo-OH/NiTe-NF	1M KOH	276	27

Tab. S2. Values of equivalent circuit elements based on EIS analysis of different electrodes.

Eletrodes	R_s (Ω)	R_{ct} (Ω)
NFF	1.12	0.47
FNO-NFF	1.12	0.23
NNO-NFF	1.11	0.20

Tab. S3. Comparison the Overall water splitting performance of NNO-NFF bifunctional electrodes to several recently reported bifunctional catalysts.

Catalyst	Electrolyte	Water splitting cell voltage (V) at 100 mA cm^{-2}	Reference
NNO-NFF	1M KOH	1.77	This work
Co-Mo-P/CoNWs	1M KOH	1.78	28
NiFe LDH-NiCoP/NF	1M KOH	1.85	29
$Ni_{0.7}Fe_{0.3}S_2$ /NF	1M KOH	1.88	30
NF/$Co_{5.0}Mo_1P$/NiFe-LDH	1M KOH	1.79	31
NiFe-LDH-Ni_3S_2/NF	1M KOH	1.89	32
Mo-Ni_2P-NiFe LDH/NF	1M KOH	1.90	33
NiFe-LDH-CoS_x/NF	1M KOH	1.96	34
$NiIr_1$ NCs	1M KOH	1.77	35
Ni_3S_2/VG-NiCo	1M KOH	1.95	36
NiCoP-NF-100	1M KOH	1.86	37

References

1. Y.-N. Zhou, Y. Ma, Z.-N. Shi, J.-C. Zhou, B. Dong, M.-X. Li, F.-G. Wang, B. Liu, J.-F. Yu and Y.-M. Chai, *Journal of Colloid and Interface Science*, 2022, **613**, 224-233.
2. Y. Ma, J. Chu, Z. Li, D. Rakov, X. Han, Y. Du, B. Song and P. Xu, *Small*, 2018, **14**, 1803783-1803789.
3. Y. Ma, H. Liu, L. Wang, C. Sun, L. Gong, J. Wang and X. Zhang, *ChemSusChem*, 2024, DOI: 10.1002/cssc.202400640.
4. C.-H. Liao, S.-F. Kang and Y.-W. Hsu, *Water Research*, 2003, **37**, 4109-4118.
5. X. Kong, C. Zhang, S. Y. Hwang, Q. Chen and Z. Peng, *Small*, 2017, **13**, 1700334-1700343a.
6. S. Anantharaj, P. E. Karthik and S. Kundu, *Catalysis Science & Technology*, 2017, **7**, 882-893.
7. H. Wang, Z. Zhao, Z. Xu, L. Li and S. Lin, *Dalton Transactions*, 2023, **52**, 1113-1121.
8. H. Wang, Z. Zhao, Z. Xu, L. Li and S. Lin, *Dalton Trans*, 2023, **52**, 1113-1121.
9. W. Wang, Q. Wen, D. Huang, Y. Lin, N. Zhao, L. Tang, M. Li, Y. Liu and R. He, *Angewandte Chemie International Edition*, 2024, DOI: 10.1002/anie.202415132.
10. H. T. Le, D. T. Tran, T. H. Nguyen, V. A. Dinh, N. H. Kim and J. H. Lee, *Applied Catalysis B: Environmental*, 2022, **317**, 121684-121693.
11. F. Lu, Y. Ji, D. Shi, P. Zhang, S. Zhang, S. Wang and B. Zhang, *Journal of Energy Storage*, 2024, **84**, 110628-110640.
12. L. Wang, Z. H. Dong, Z. G. Wang, F. X. Zhang and J. Jin, *Advanced Functional Materials*, 2012, **23**, 2758-2764.
13. D. Cheng, Q. Zhong, Y. Xiong, Y. Bu and J. Wang, *Journal of Alloys and Compounds*, 2020, **817**, 152689-125696.
14. Y. Ma, J. Chu, Z. Li, D. Rakov, X. Han, Y. Du, B. Song and P. Xu, *Small*, 2018, **14**, 1803783-1803789.
15. Z. Xiao, Y.-C. Huang, C.-L. Dong, C. Xie, Z. Liu, S. Du, W. Chen, D. Yan, L. Tao, Z. Shu, G. Zhang, H. Duan, Y. Wang, Y. Zou, R. Chen and S. Wang, *Journal of the American Chemical Society*, 2020, **142**, 12087-12095.
16. C. E. Chukwuneke, K. Kawashima, H. Li, R. A. Marquez, Y. J. Son, L. A. Smith, H. Celio, G. Henkelman and C. B. Mullins, *Journal of Materials Chemistry A*, 2024, **12**, 1654-1661.
17. Z. Zou, Z. Zheng, Y. Chen, Y. Shao, X. Zheng, C. Zhao and Q. Wang, *Inorganic Chemistry Frontiers*, 2024, **11**, 837-844.
18. C. Wan, J. Jin, X. Wei, S. Chen, Y. Zhang, T. Zhu and H. Qu, *Journal of Materials Science & Technology*, 2022, **124**, 102-108.
19. H. Yang, L. Ge, J. Guan, B. Ouyang, H. Li and Y. Deng, *J Colloid Interface Sci*, 2024, **653**, 721-729.
20. Y. Mei, Y. Feng, C. Zhang, Y. Zhang, Q. Qi and J. Hu, *ACS Catalysis*, 2022, **12**, 10808-10817.
21. M. Wang, Y. Chen, Z. Yu, Y. Hou, R. Jiang, S. Li, J. Chen, W. Tang, H. Pang and W. Xie, *J Colloid Interface Sci*, 2023, **640**, 1-14.
22. C. Wang, K. Li, M. Zhao, Z. Li and J. Zheng, *Separation and Purification Technology*, 2024, **340**, 126641-126650.
23. S. Wang, X. Ning, Y. Cao, R. Chen, Z. Lu, J. Hu, J. Xie and A. Hao, *Inorg Chem*, 2023, **62**, 6428-6438.
24. Y. Guo, X. Zou, X. Wei, W. Bao, J. Zhang, J. Han and F. Jia, *Chinese Journal of Structural*

Chemistry, 2024, **43**, 100206-100212.

25. L. Xu, P. Yang, R. Ye, X. Wu and Y. Tao, *Journal of Materials Chemistry A*, 2024, **12(16)**, 9714-9722.
26. J. Feng, C. Chu, J. Liu, L. Wei, H. Li and J. Shen, *International Journal of Hydrogen Energy*, 2024, **63**, 231-240.
27. J. Liu, D. Liu, X. Yan, P. Guo, H. Xu, P. Chen and R. Wu, *Journal of Materials Chemistry A*, 2024, **12(22)**, 13160-13167.
28. V. H. Hoa, D. T. Tran, D. C. Nguyen, D. H. Kim, N. H. Kim and J. H. Lee, *Advanced Functional Materials*, 2020, **30**, 2002533-2002544.
29. H. Zhang, X. Li, A. Hähnel, V. Naumann, C. Lin, S. Azimi, S. L. Schweizer, A. W. Maijenburg and R. B. Wehrspohn, *Advanced Functional Materials*, 2018, **28**, 1706847-1706856.
30. J. Yu, G. Cheng and W. Luo, *Journal of Materials Chemistry A*, 2017, **5**, 15838-15844.
31. W. Mai, Q. Cui, Z. Zhang, K. Zhang, G. Li, L. Tian and W. Hu, *ACS Applied Energy Materials*, 2020, **3**, 8075-8085.
32. L. Ren, C. Wang, W. Li, R. Dong, H. Sun, N. Liu and B. Geng, *Electrochimica Acta*, 2019, **318**, 42-50.
33. Z. Yang, Y. Lin, F. Jiao, J. Li, J. Wang and Y. Gong, *Journal of Energy Chemistry*, 2020, **49**, 189-197.
34. Y. Yang, Y. Xie, Z. Yu, S. Guo, M. Yuan, H. Yao, Z. Liang, Y. R. Lu, T.-S. Chan, C. Li, H. Dong and S. Ma, *Chemical Engineering Journal*, 2021, **419**, 129512-129521.
35. Z. Cai, P. Wang, X. Zhao, X. Bu, J. Zhang, Y. Chen, J. Xu, Y. Yan, A. Chen and X. Wang, *RSC Adv*, 2023, **13**, 17315-17323.
36. X. Zhang, J. Fan, X. Lu, Z. Han, C. Cazorla, L. Hu, T. Wu and D. Chu, *Chemical Engineering Journal*, 2021, **415**, 129048-129058.
37. L. Chen, Y. Song, Y. Liu, L. Xu, J. Qin, Y. Lei and Y. Tang, *Journal of Energy Chemistry*, 2020, **50**, 395-401.